Role of foreign phases, synergistic effects, and morphology in the HER performance of trimetallic pentlandites with unequimolar Co:Fe:Ni ratio

Maciej Kubowicz, Miłosz Kożusznik, Tomasz Kurek, Krzysztof Mars and Andrzej Mikuła*

Faculty of Materials Science and Ceramics, AGH University of Krakow, al. Mickiewicza 30-059 Krakow, Poland
* Correspondence: amikula@agh.edu.pl

Abstract: Since pentlandites are among the most promising catalysts for hydrogen evolution reactions (HER), in this study, we investigated the influence of different cobalt, iron, and nickel substitutions in the cationic sublattice and the form of the material (powder, ingot, sintered pellet) on catalytic performance. This complements previous results regarding a multi-component approach in these chalcogenides. It was shown that in the case of sulfur-rich pentlandites with non-equimolar ratio of Co, Fe, and Ni, the impact of intrinsic material properties is smaller than surface-related effects. Among powder forms, catalysts based on a combination of Fe and Co perform the best. However, in volumetric forms, extremely high contents of individual metals are favorable, albeit associated with active precipitations of foreign phases. The presence of these phases positively affects the recorded currents but slows down the reaction kinetics. These findings shed light on the nuanced interplay between material composition, form, and HER properties, offering insights for tailored catalyst design.

1. Sample preparation and structural measurements

The materials post-synthesis were proceed into working electrodes in three forms: powders, ingots, and sintered pellets. The obtained ingots were either ground into powder or suitable flat fragments were cut out from them. The powders were also used to craft sintered pellets. The grain size analysis of the powder particles after normalized grinding procedure is presented in Figure S1.

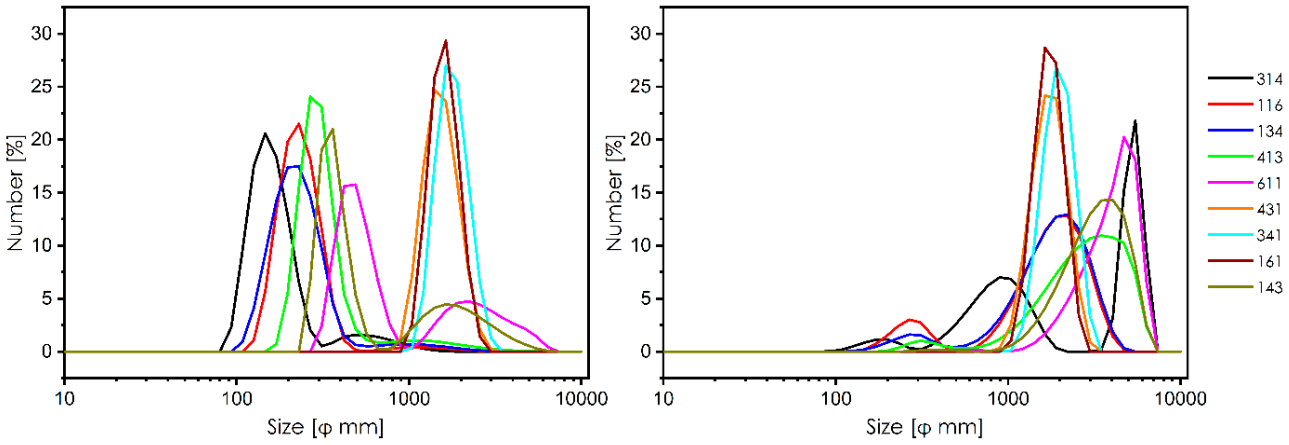

Figure S1. DLS results of the particles size as a function of (a) number and (b) volume distribution.

Powder catalysis preparation. The powder on the screen-printable electrodes was applied from a mixture of: 7.5 mg powder; 1050 μm distilled water; 300 μm isopropanol; 150 μm nafion D-520 dispersion, and then sonicated for 20 minutes. Approximately 4 μl of the sample solution was then applied by drop-casting to a screen-printing electrode and left to dry. Figure S2 shows microscopic images (taken by *Olympus SZX7 optical microscope*) of each of the applied samples.

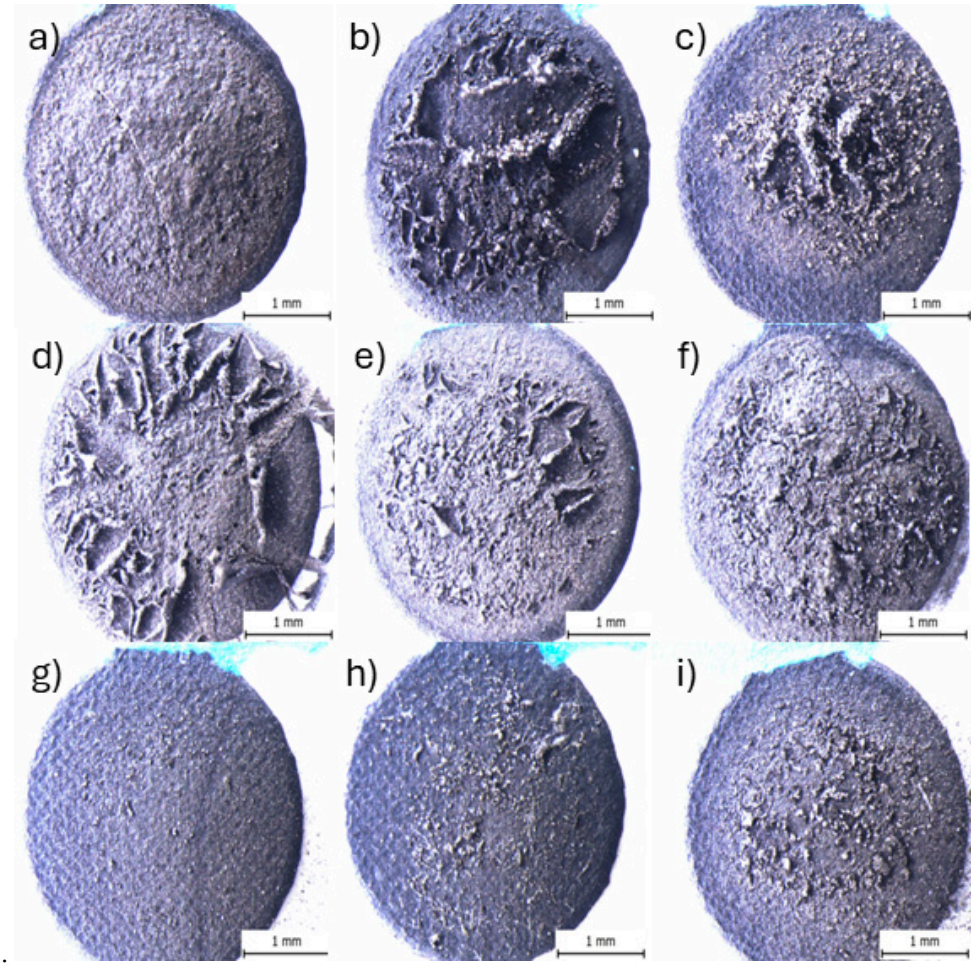

Figure S2. Photos of powders applied to screen-printable electrodes (a) Po314; (b) Po116; (c) Po134; (d) Po413; (e) Po611; (f) Po431; (g) Po341; (h) Po161; (i) Po143.

Ingots and pellets catalysis preparation. Prior to electrochemical measurements, the ingots and pellets were carefully polished using sandpaper and Al_2O_3 polishing paste. An electrode was then constructed from each sample by attaching the sample directly to a platinum wire and placing it in a glass holder, then using silicone to isolate the wire from access to the electrolyte.

Inductive Hot Pressing (IHP) consolidating process. The powders were inserted into graphite molds and sintered by using of custom-made apparatus. The process was carried out under the following conditions: rinsing with Argon (0.5 atm) at room temperature; heating to 200 [°C] with a heating rate of 100 [°C/min]; annealing at this temperature for 5 minutes to eliminate stresses; heating to 400 [°C] with a heating rate of [°C/min]; annealing at this temperature for 14 minutes with applied pressure of 50 [MPa] and 1 minute

without pressure; cooling to room temperature. The powders were consolidated into pellets with a diameter of 10 [mm] and height of about 0.3 [cm]. These are standard conditions we have used in our previous studies on pentlandites, facilitating comparability [30,31].

The density of the as-sintered pellets and ingots are presented in Table S1. The density was estimated using Archimedes principle.

Table S1. Density of the ingot and sintered pellet samples

Sample	In314	In116	In134	In413	In611	In431	In341	In161	In143
Relative density [%]	90,77	91,43	91,68	95,02	90,08	88,69	87,31	85,24	89,92
Sample	Pe314	Pe116	Pe134	Pe413	Pe611	Pe431	Pe341	Pe161	Pe143
Relative density [%]	88,14	92,87	86,38	92,77	79,84	80,52	84,56	91,08	83,46

Structural investigation. A summary of the phase composition together with fitting parameters are presented in the main article. Scanning Electron Microscope (SEM) micrographs, together with elements distribution at the respective surfaces (EDX) for all materials' form are presented in Figures S3–S5.

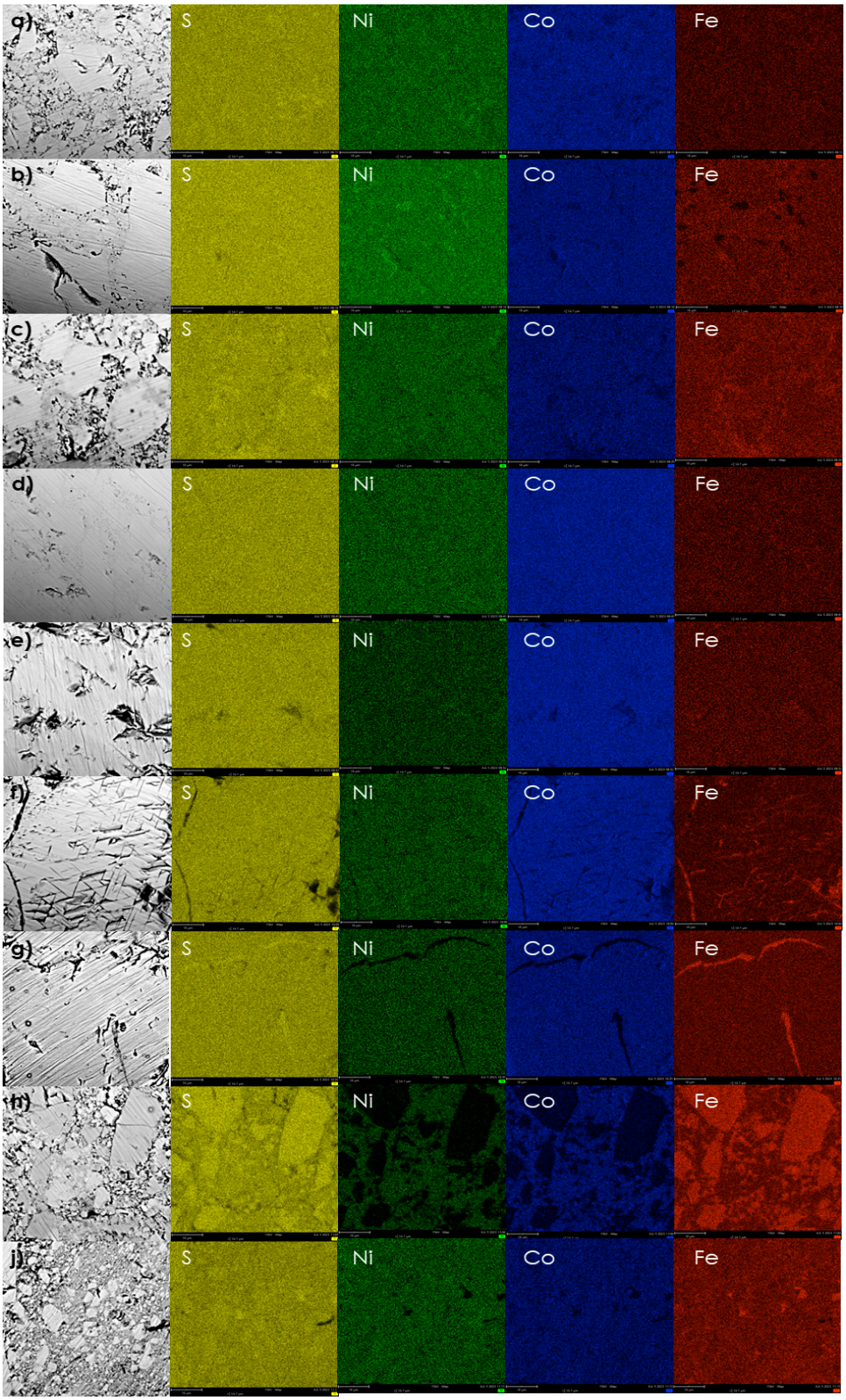

Figure S3. SEM micrographs together with EDX mapping for: (a) Pe314; (b) Pe116; (c) Pe134; (d) Pe413; (e) Pe611; (f) Pe431; (g) Pe341; (h) Pe161; (i) Pe143.

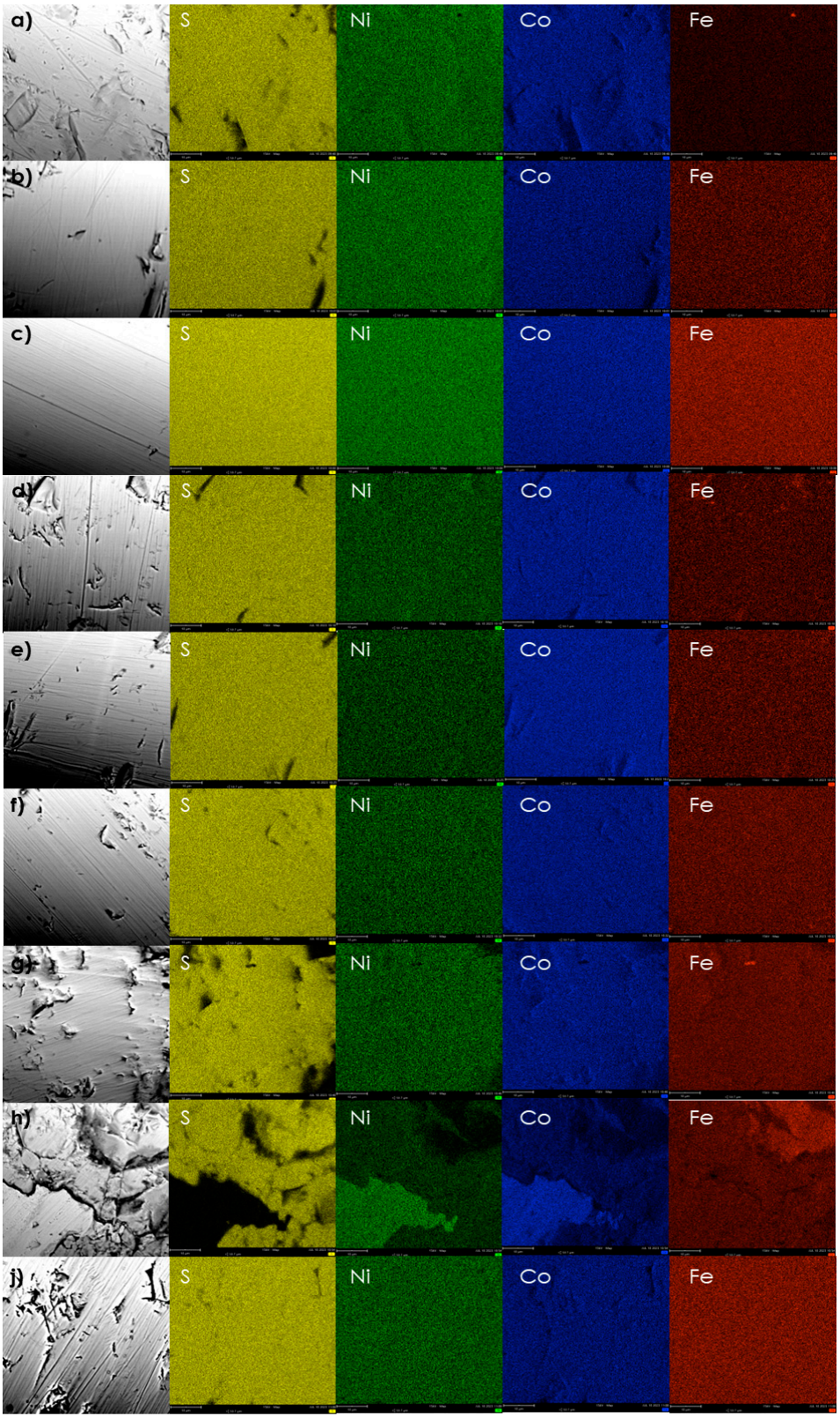

Figure S4. SEM micrographs together with EDX mapping for: (a) In314; (b) In116; (c) In134; (d) In413; (e) In611; (f) In431; (g) In341; (h) In161; (i) In143.

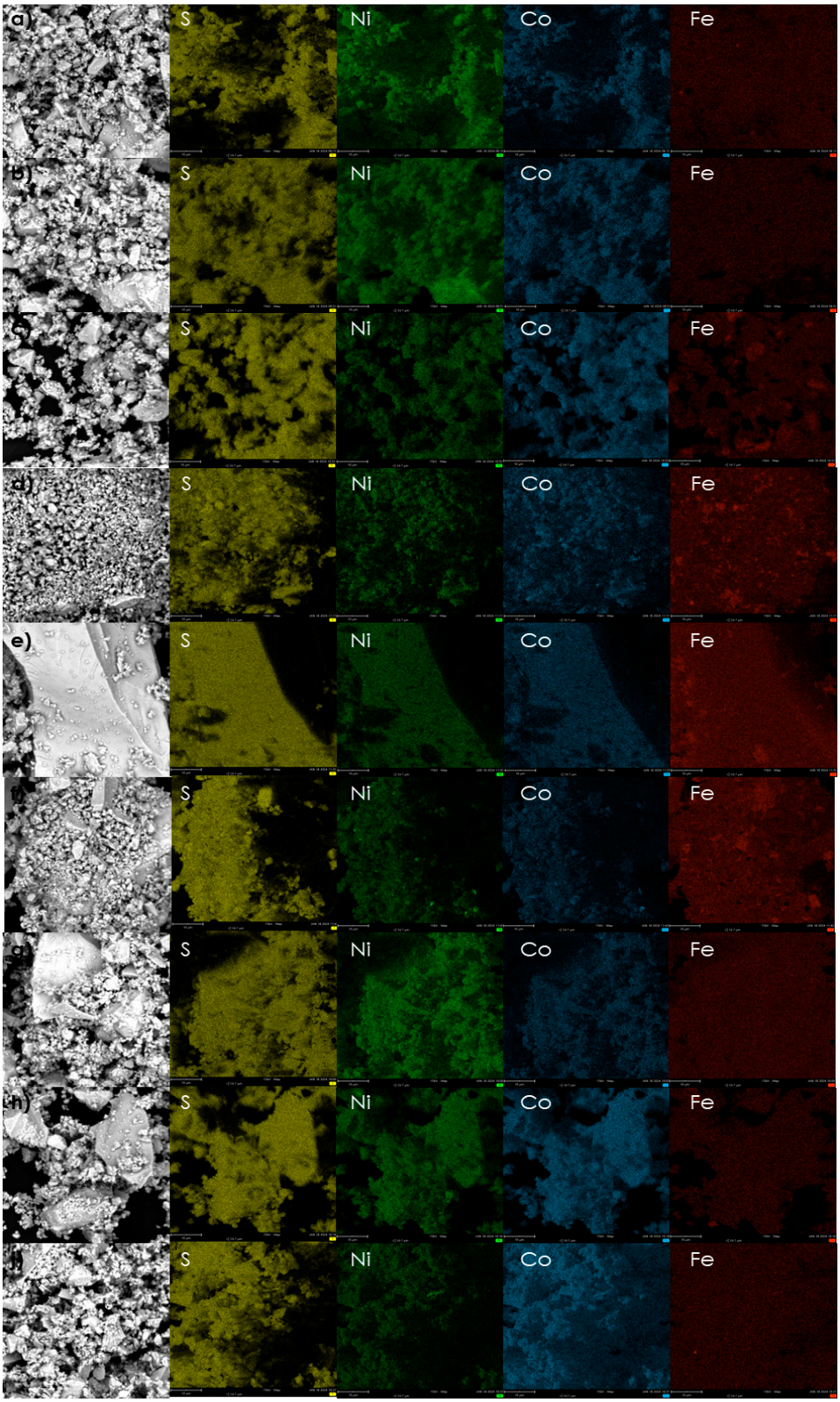

Figure S5. SEM micrographs together with EDX mapping for: (a) Po314; (b) Po116; (c) Po134; (d) Po413; (e) Po611; (f) Po431; (g) Po341; (h) Po161; (i) Po143.

Table S2. The summary of the chemical and phase compositions of the considered materials, along with the fitting parameters.

Name of sample	Nominal chemical composition	Estimated chemical composition (ICP-OES)	Estimated chemical composition (EDX)	GoF	Other phases in material	wRp
Po314	$Co_3Fe_{1.5}Ni_{4.5}S_8$	$Co_{3.11}Fe_{1.46}Ni_{5.93}S_8$	$Co_{2.39}Fe_{1.34}Ni_{4.27}S_8$	1.26	-	2.61
In314			$Co_{2.98}Fe_{1.52}Ni_{4.49}S_8$			
Pe314		$Co_{3.37}Fe_{1.67}Ni_{5.07}S_8$	$Co_{3.07}Fe_{1.46}Ni_{4.47}S_8$	1.72	4% Fe	3.30
Po116	$Co_{1.5}Fe_{1.5}Ni_6S_8$	$Co_{1.72}Fe_{1.66}Ni_{6.94}S_8$	$Co_{1.62}Fe_{1.47}Ni_{5.90}S_8$	3.40	3,7% NiS	5.55
In116			$Co_{1.55}Fe_{1.56}Ni_{5.89}S_8$			
Pe116		$Co_{1.47}Fe_{1.45}Ni_{6.01}S_8$	$Co_{1.61}Fe_{1.54}Ni_{5.85}S_8$	6,33	12,1% NiS	7.06
Po134	$Co_{1.5}Fe_3Ni_{4.5}S_8$	$Co_{1.76}Fe_{3.64}Ni_{5.19}S_8$	$Co_{1.59}Fe_{3.06}Ni_{4.36}S_8$	1.37	-	3.08
In134			$Co_{1.51}Fe_{2.93}Ni_{4.56}S_8$			
Pe134		$Co_{1.54}Fe_{2.97}Ni_{4.63}S_8$	$Co_{1.52}Fe_{3.07}Ni_{4.41}S_8$	1.77	3% Fe	3.54
Po413	$Co_{4.5}Fe_{1.5}Ni_3S_8$	$Co_{4.65}Fe_{1.29}Ni_{4.70}S_8$	$Co_{4.51}Fe_{1.46}Ni_{3.03}S_8$	1.58	-	2.91
In413			$Co_{4.41}Fe_{1.51}Ni_{3.01}S_8$			
Pe413		$Co_{1.54}Fe_{2.97}Ni_{4.63}S_8$	$Co_{4.47}Fe_{1.52}Ni_{3.01}S_8$	1.91	-	3.05
Po611	$Co_6Fe_{1.5}Ni_{1.5}S_8$	$Co_{6.66}Fe_{1.16}Ni_{2.57}S_8$	$Co_{5.99}Fe_{1.54}Ni_{1.47}S_8$	1.09	-	2.55
In611			$Co_{5.95}Fe_{1.50}Ni_{1.55}S_8$			
Pe611		$Co_{6.05}Fe_{1.63}Ni_{1.47}S_8$	$Co_{5.93}Fe_{1.56}Ni_{1.51}S_8$	1.28	-	2.56
Po431	$Co_{4.5}Fe_3Ni_{1.5}S_8$	$Co_{5.15}Fe_{3.07}Ni_{2.26}S_8$	$Co_{4.53}Fe_{2.96}Ni_{1.51}S_8$	1.25	-	2.95
In431			$Co_{4.68}Fe_{2.75}Ni_{1.57}S_8$			
Pe431		$Co_{4.48}Fe_{3.06}Ni_{1.51}S_8$	$Co_{4.15}Fe_{2.35}Ni_{1.50}S_8$	1.03	15,3% Pyrrohotite (FeS)	2.25
Po341	$Co_3Fe_{4.5}Ni_{1.5}S_8$	$Co_{3.72}Fe_{5.41}Ni_{1.87}S_8$	$Co_{3.15}Fe_{4.51}Ni_{1.34}S_8$	1.51	5,7% Pyrrhotite (FeS)	2.83
In341			$Co_{3.42}Fe_{3.85}Ni_{1.75}S_8$			
Pe341		$Co_{3.24}Fe_{5.08}Ni_{1.55}S_8$	$Co_{2.94}Fe_{3.42}Ni_{1.63}S_8$	1.07	22% Troilite (FeS)	2.46
Po161	$Co_{1.5}Fe_6Ni_{1.5}S_8$	$Co_{1.69}Fe_{7.27}Ni_{1.59}S_8$	$Co_{1.66}Fe_{6.03}Ni_{1.31}S_8$	1.60	4,8% Fe + 24,3% Troilite (FeS)	2.64
In161			$Co_{1.46}Fe_{5.29}Ni_{2.25}S_8$			
Pe161		$Co_{1.72}Fe_{7.39}Ni_{1.68}S_8$	$Co_{1.25}Fe_{5.58}Ni_{1.16}S_8$	1.62	35,3% Troilite (FeS) + 11,3% Pyrrhotitie (FeS)	2.64
Po143	$Co_{1.5}Fe_{4.5}Ni_3S_8$	$Co_{1.81}Fe_{5.05}Ni_{3.97}S_8$	$Co_{1.67}Fe_{4.71}Ni_{2.62}S_8$	2.12	-	3.63
In143			$Co_{1.59}Fe_{4.08}Ni_{3.33}S_8$			
Pe143		$Co_{1.52}Fe_{4.87}Ni_{3.00}S_8$	$Co_{1.38}Fe_{3.99}Ni_{2.63}S_8$	1.26	16,9% Pyrrhotite (FeS)	2.79

2. Theoretical investigation.

The lattice constants as well as formation energy are presented in Table S2. After the relaxation process the volume changes up to 2% - increasing with the addition of Ni and decreases when adding either Fe or Co.

Table S3. Structural parameters as well as formation energies calculated for pentlandites and the elements building the pentlandite structure.

Material	a [Å]	b [Å]	c [Å]	α [°]	β [°]	γ [°]	V [Å^3]	ΔE_{form} [eV/at]
Pentlandites								
Initial	9.84000	-	-	90.0000	-	-	952.7639	-
$Co_3Fe_{1.5}Ni_{4.5}S_8$	9.87591	9.87590	9.88340	90.0355	90.0930	89.9451	963.9600	-1.0608
$Co_{1.5}Fe_{1.5}Ni_6S_8$	9.92606	9.92879	9.93970	89.9545	89.9549	89.8688	979.5927	-1.0388
$Co_{1.5}Fe_3Ni_{4.5}S_8$	9.86957	9.86644	9.87559	89.9667	90.0900	89.8876	961.6562	-1.0673
$Co_{4.5}Fe_{1.5}Ni_3S_8$	9.82923	9.83280	9.83841	89.9859	89.9656	89.9263	950.8699	-1.0774
$Co_6Fe_{1.5}Ni_{1.5}S_8$	9.81582	9.81333	9.81136	89.9973	89.9766	89.9027	945.0862	-1.0830
$Co_{4.5}Fe_3Ni_{1.5}S_8$	9.79053	9.79629	9.80633	90.0394	90.0194	90.0363	940.5334	-1.0711
$Co_3Fe_{4.5}Ni_{1.5}S_8$	9.78376	9.78910	9.84084	89.4171	89.5453	89.4484	942.3773	-1.0540
$Co_{1.5}Fe_6Ni_{1.5}S_8$	9.82972	9.84025	9.85555	89.2301	90.7614	90.9953	952.9865	-1.0271
$Co_{1.5}Fe_{4.5}Ni_3S_8$	9.81236	9.80873	9.84771	89.6910	89.6808	89.6345	947.7622	-1.0649
Elements								
							Co	-7.04789
							Fe	-8.24819
							Ni	-5.48319
							S	-4.10876

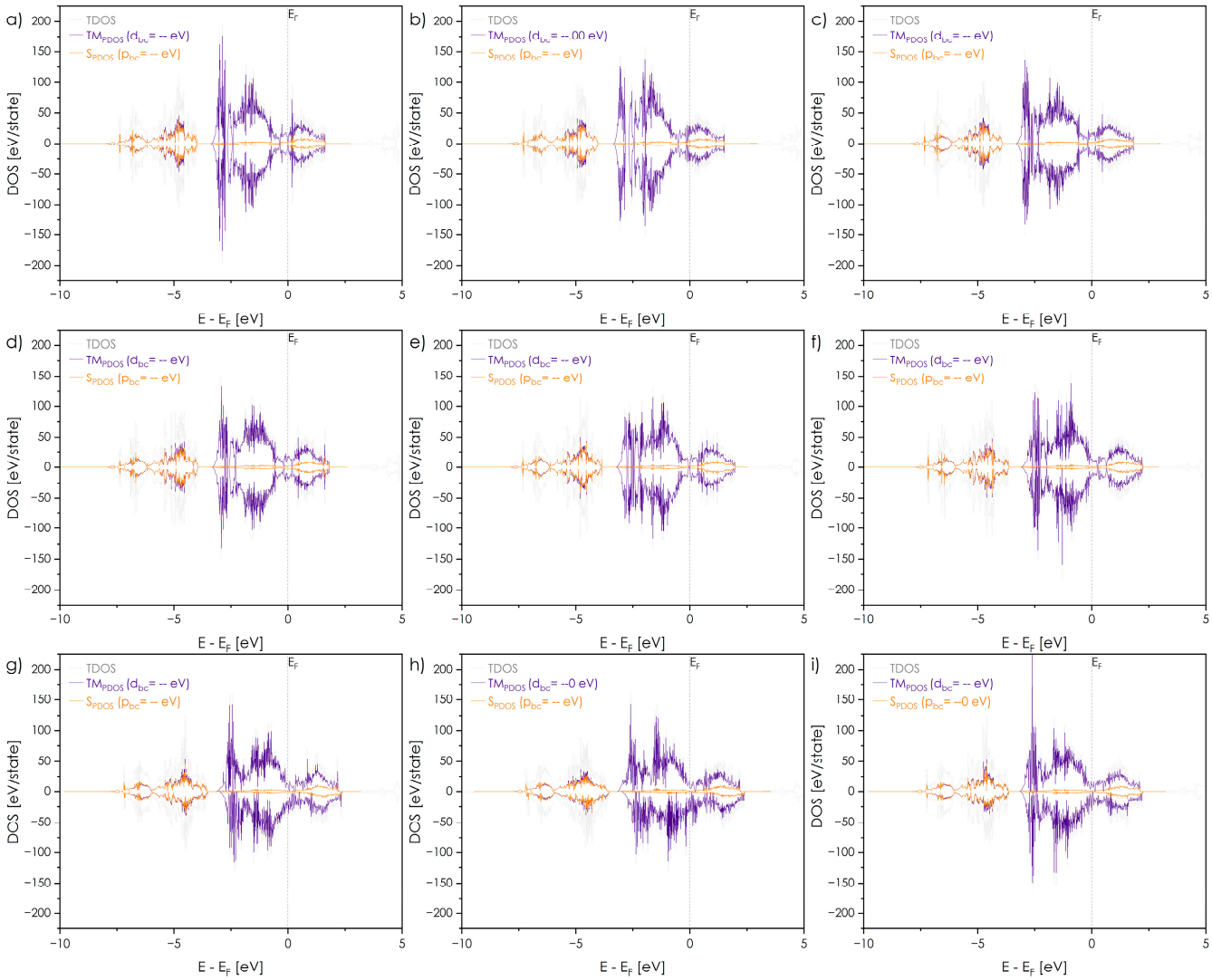

Figure S6. Total and partial density of states of examined materials: “314” (a), “116” (b), “134” (c), “413” (d), “611” (e), “431” (f), “341” (g), “161” (h), “143” (i).

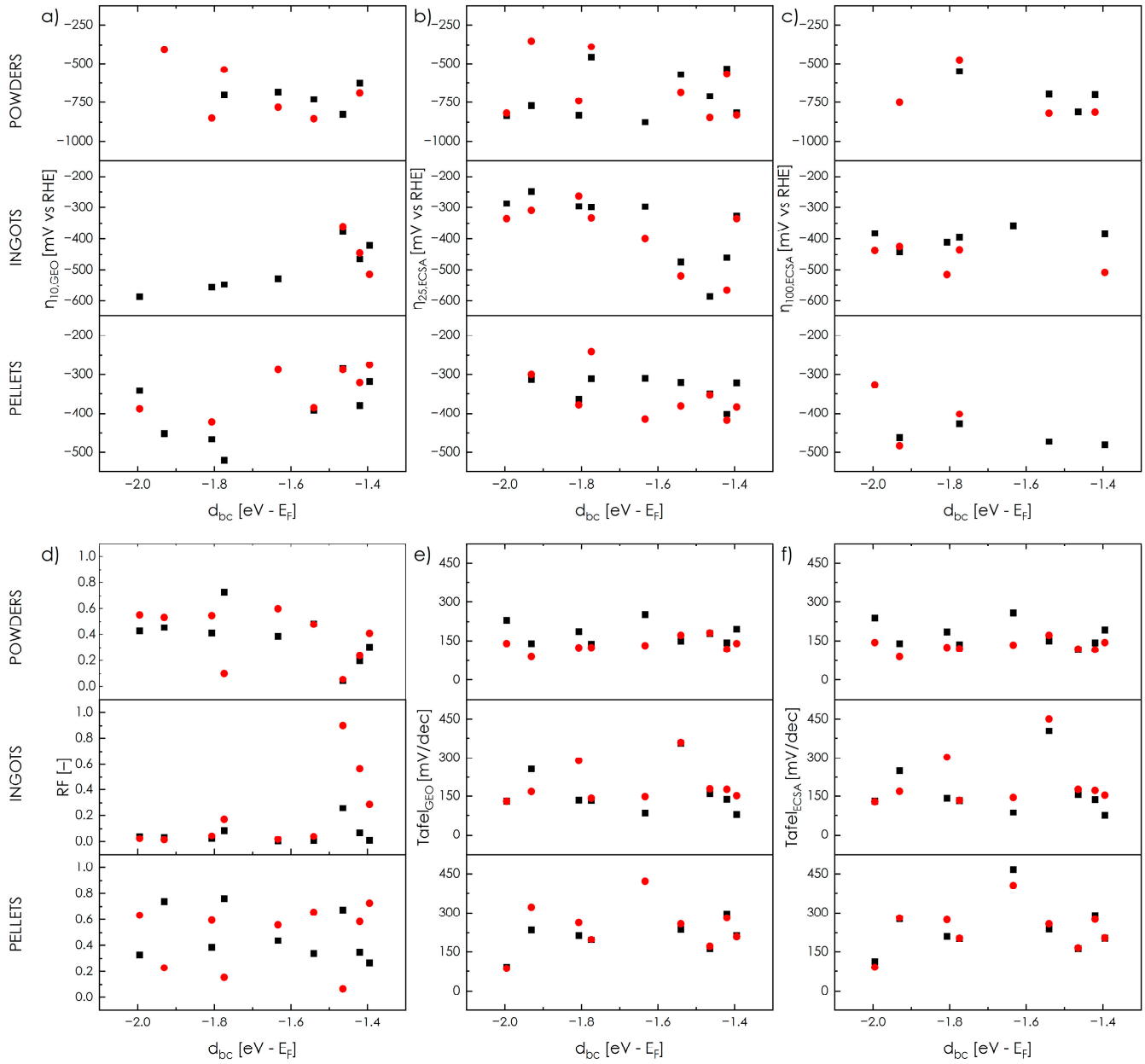

Figure S7. Benchmarking parameters as a function of calculated d_{bc} of examined materials: overpotential: at 10 mA/cm^2 normalized to geometric area (a), at 25 mA/cm^2 normalized to ECSA (b), at 100 mA/cm^2 normalized to ECSA (c); roughness factor (d), Tafel slope for current densities normalized to geometric area (e) and ECSA (f).

3. Electrochemical testing

Electrochemical measurements procedure. Linear sweep voltammetry (LSV) measurements were conducted in a three-electrode system, with a powder/ingot/pellet acting as working electrode, a platinum black electrode (Pt + Pt black) as a counter-electrode, and a silver chloride electrode (Ag/AgCl 3M KCl) as a reference electrode respectively. Measurements were performed in 0.5M H_2SO_4 as electrolyte on electrochemical measurement equipment (*MTM-ANKO*) at room temperature.

The electrochemical measurement was divided into several steps. The first was electrochemical cleaning of the electrode surface, by measuring the linear sweep voltammetry (LSV) twenty times in the potential range from -200 to 200 [mV] at a scan rate of 200 [mVs^{-1}]. This was followed by electrochemical active surface area (ECSA) measurements based on double layer capacitance (C_{dl}) measurements. For this measurement, cyclic voltammetry (CV) was used in the non-Faraday range of potential difference [mV] from a scan rate of 2.1 [mVs^{-1}] to 500 [mVs^{-1}]. This yielded a function of charge current on scan rate (denoted C_{dl}), and this value divided by specific capacitance of 0.035 [$mFcm^{-2}$] gives the ECSA value [31]. Next, the two-hour chronoamperometry measurements with a preset potential difference of -600 (-800 for powder samples) [mV] were carried out as the main indicator of materials' stability. After the stability tests, the entire LSV measurement procedure was repeated and denoted as "post". The CV measurements together with estimated C_{DL} values are presented in Figures S9–S15. Tafel Slope values were extracted from the obtained LSV measurements by logarithmizing the current density curves and performing linear fit in the potential ranges where the j-E response was linear resulting in equation (S1).

$$\log J = \log J_0 + a\eta, \qquad (S1)$$

where J_0 – exchange current density, a – Tafel slope, η – overpotential. The exchange current density as well as Tafel slope values were taken as the intercept and slope of the linear fit, respectively. The summary of recorded ECSA, roughness factor (RF), the overpotentials at certain current densities and normalized to ECSA or geometric area, estimated Tafel slope values, and J_0 are presented in Tables S4–S6.

Electrical impedance spectroscopy (EIS) measurements were carried out to determine the charge transfer resistance (R_{CT}) and presented in Table S6. The model used in this study was a circuit consisting of a resistor, a capacitor and a Warburg element, and the measurement itself was carried out between 1 [Hz] and 50 [kHz]. These measurements were carried out on a *Gamry Interface 1010E*. As can be seen in **Error! Reference source not found.**, the resistance of the sintered samples (Pellet) is an order of magnitude lower than that of the merely synthesized samples (Ingot), and especially compared to powder samples. The smallest decrease was recorded for the most multi-phase material, which is due to the new pseudo-FeS phases precipitated in the material. For the other materials, a significant decrease in resistivity can be observed after the IHP sintering process. The materials studied have significant charge carrier density and cation mobility, and sintering densifies the material and further improves the mobility of carriers within the grains [9] [9]. The relationship of the proportion of individual transition metals to the resistance of the samples can also be seen. In samples where the proportion of iron is predominant (In431, In341, In161, In143), the resistance is noticeably lower than in other samples. An inverse relationship can be observed in samples with predominantly nickel. After sintering, no definite relationship can be seen, which is due to the precipitation of new phases in the material, and the results themselves are close to the error limit. The powder samples were deposited on screen-printed electrodes, so their results are affected by the substrate.

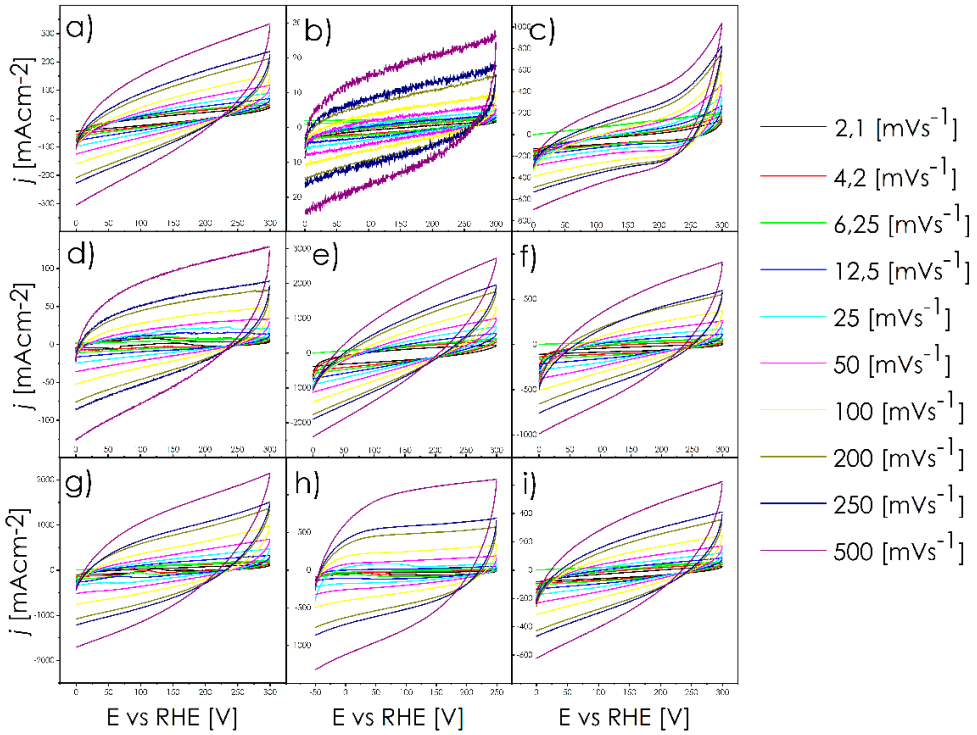

Figure S82. CV voltammograms witch different scan rates for determining ECSA before/after stability tests for "pre" (a) Pe314; (b) Pe116; (c) Pe134; (d) Pe413; (e) Pe611; (f) Pe431; (g) Pe341; (h) Pe161; (i) Pe143.

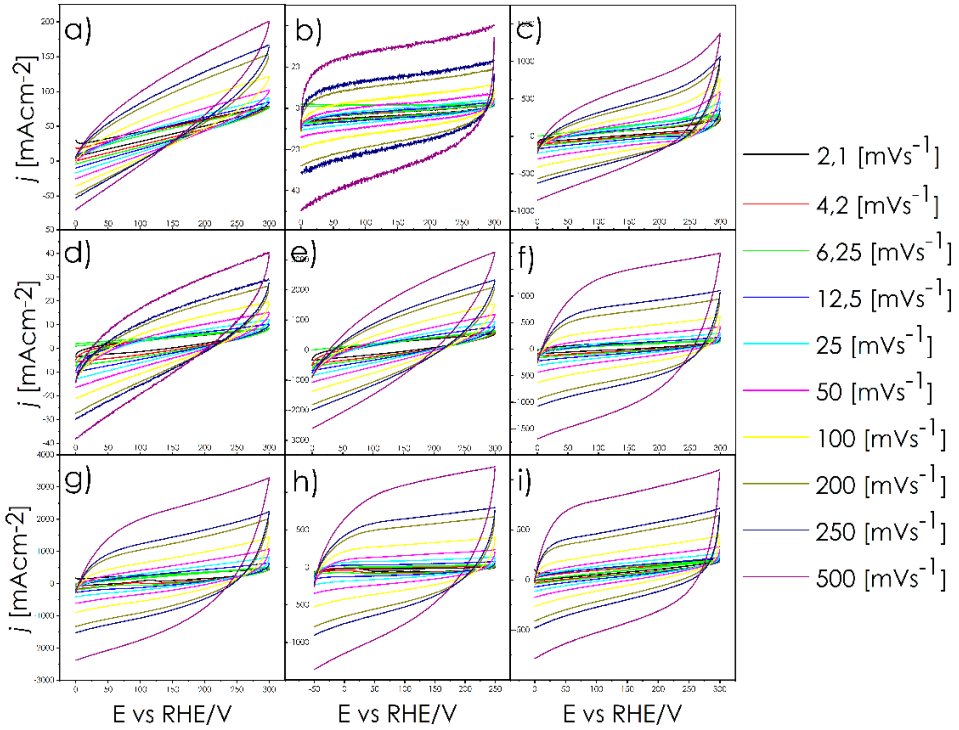

Figure S93. CV voltammograms witch different scan rates for determining ECSA before/after stability tests for "post" (a) Pe314; (b) Pe116; (c) Pe134; (d) Pe413; (e) Pe611; (f) Pe431; (g) Pe341; (h) Pe161; (i) Pe143.

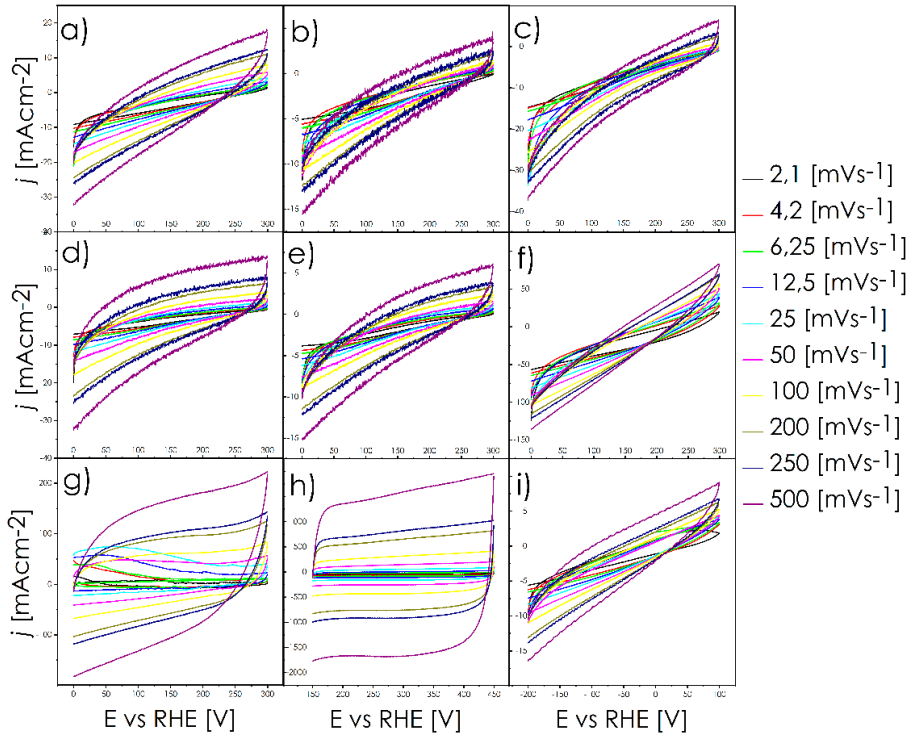

Figure S104. CV voltammograms witch different scan rates for determining ECSA before/after stability tests for "pre" (a) In314; (b) In116; (c) In134; (d) In413; (e) In611; (f) In431; (g) In341; (h) In161; (i) In143.

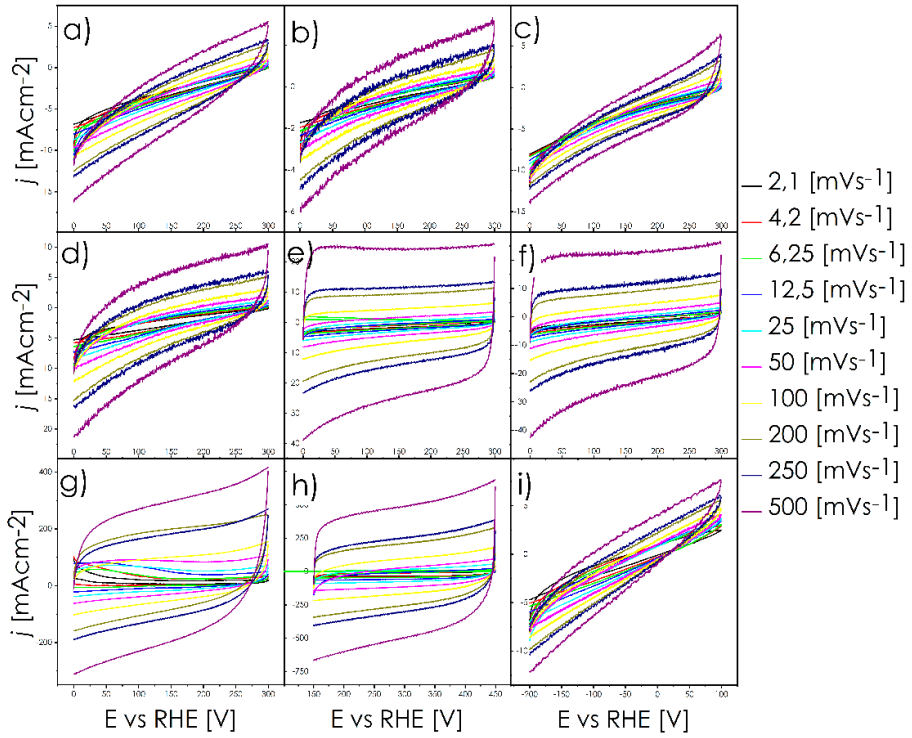

Figure S115. CV voltammograms witch different scan rates for determining ECSA before/after stability tests for "post" (a) In314; (b) In116; (c) In134; (d) In413; (e) In611; (f) In431; (g) In341; (h) In161; (i) In143.

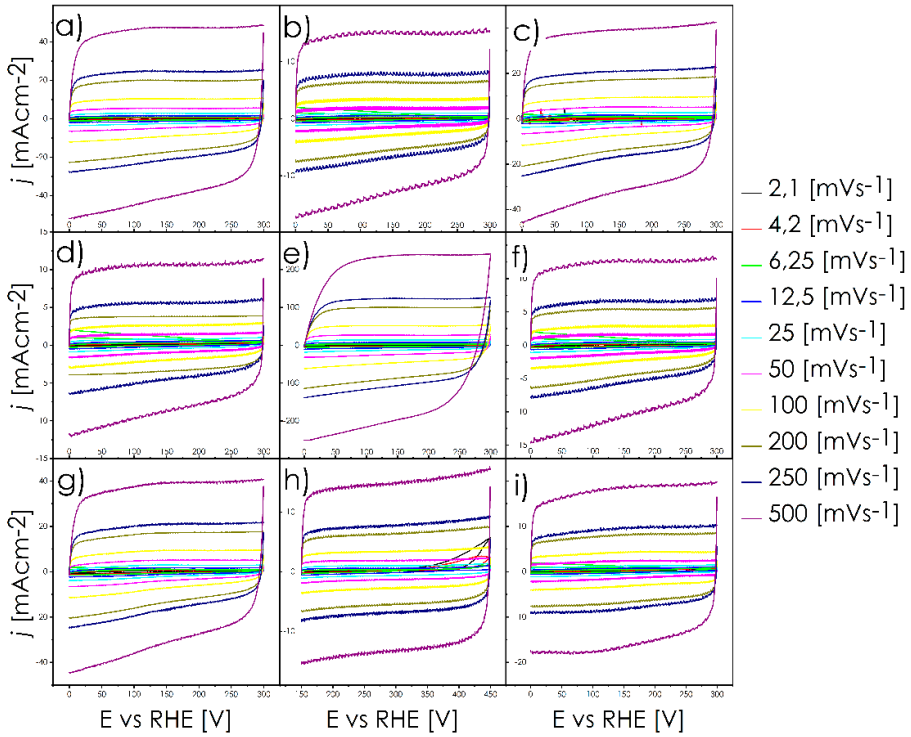

Figure S126. CV voltammograms witch different scan rates for determining ECSA before/after stability tests for "pre" (a) Po314; (b) Po116; (c) Po134; (d) Po413; (e) Po611; (f) Po431; (g) Po341; (h) Po161; (i) Po143.

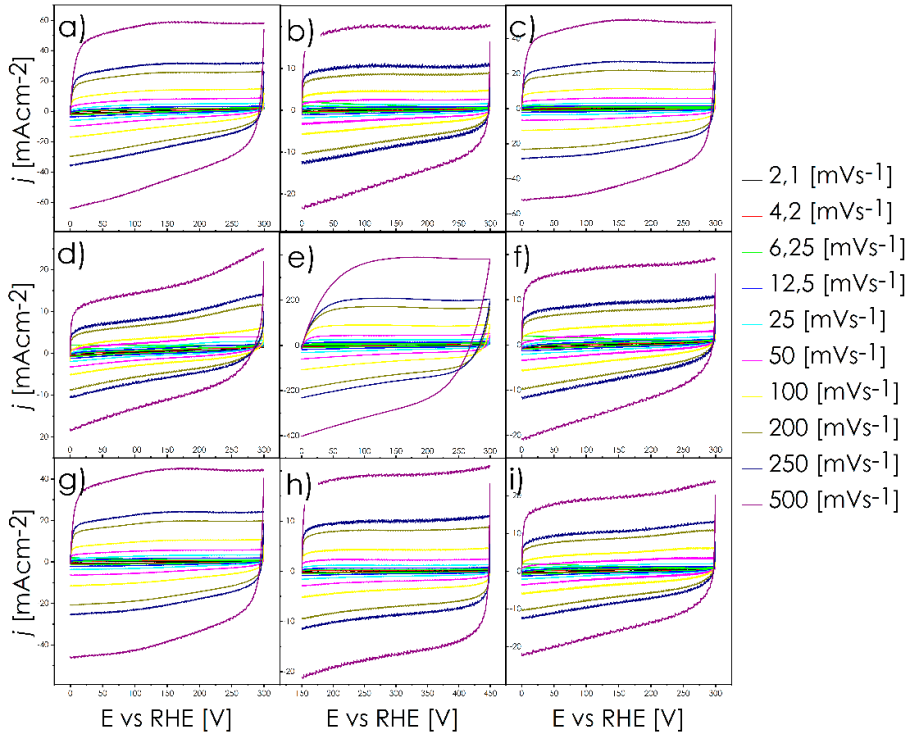

Figure S137. CV voltammograms witch different scan rates for determining ECSA before/after stability tests for "post" (a) Po314; (b) Po116; (c) Po134; (d) Po413; (e) Po611; (f) Po431; (g) Po341; (h) Po161; (i) Po143.

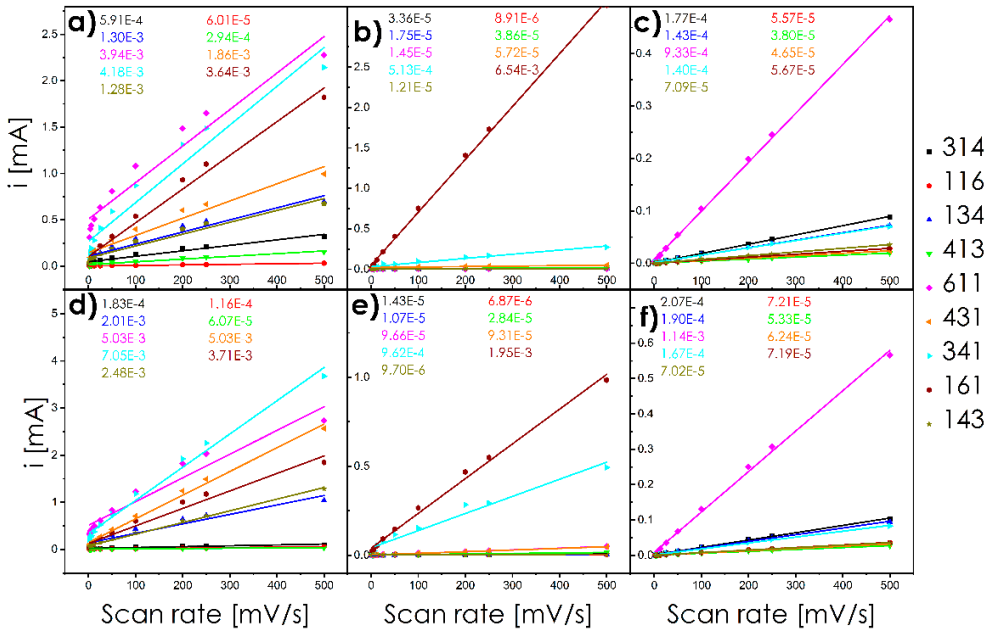

Figure S148. Charging current densities representing C_{dl} values for (a) pellets before chronoamperometry; (b) ingots before chronoamperometry; (c) powders before chronoamperometry; (d) pellets after chronoamperometry; (e) ingots after chronoamperometry; (f) powders after chronoamperometry.

Table S4. ECSA and RF values for all samples before and after the stability tests.

Sample	Working area [cm²]	Samples "pre"		Samples "post"		Activation process
		ECSA [cm²]	RF (-)	ECSA [cm²]	RF (-)	
Pe314	$156.07 \cdot 10^{-3}$	$1{,}69 \cdot 10^{-2}$	$1{,}08 \cdot 10^{-1}$	$5{,}21 \cdot 10^{-3}$	$3{,}34 \cdot 10^{-2}$	-
Pe116	$120.80 \cdot 10^{-3}$	$1{,}72 \cdot 10^{-3}$	$1{,}42 \cdot 10^{-2}$	$3{,}32 \cdot 10^{-3}$	$2{,}75 \cdot 10^{-2}$	+
Pe134	$217.34 \cdot 10^{-3}$	$3{,}72 \cdot 10^{-2}$	$1{,}71 \cdot 10^{-1}$	$5{,}73 \cdot 10^{-2}$	$2{,}64 \cdot 10^{-1}$	+
Pe413	$217.76 \cdot 10^{-3}$	$8{,}59 \cdot 10^{-3}$	$3{,}94 \cdot 10^{-2}$	$1{,}74 \cdot 10^{-3}$	$8{,}01 \cdot 10^{-3}$	-
Pe611	$186.05 \cdot 10^{-3}$	$1{,}13 \cdot 10^{-1}$	$6{,}05 \cdot 10^{-1}$	$1{,}44 \cdot 10^{-1}$	$7{,}73 \cdot 10^{-1}$	+
Pe431	$127.00 \cdot 10^{-3}$	$5{,}31 \cdot 10^{-2}$	$4{,}18 \cdot 10^{-1}$	$1{,}44 \cdot 10^{-1}$	1,13	+
Pe341	$250.66 \cdot 10^{-3}$	$1{,}19 \cdot 10^{-1}$	$4{,}77 \cdot 10^{-1}$	$2{,}01 \cdot 10^{-1}$	$8{,}04 \cdot 10^{-1}$	+
Pe161	$113.56 \cdot 10^{-3}$	$1{,}14 \cdot 10^{-1}$	$9{,}15 \cdot 10^{-1}$	$1{,}06 \cdot 10^{-1}$	$0{,}93 \cdot 10^{-1}$	-
Pe143	$181.35 \cdot 10^{-3}$	$3{,}65 \cdot 10^{-2}$	$2{,}01 \cdot 10^{-1}$	$7{,}08 \cdot 10^{-2}$	$3{,}90 \cdot 10^{-1}$	+
In314	$187.87 \cdot 10^{-3}$	$9{,}61 \cdot 10^{-4}$	$5{,}12 \cdot 10^{-3}$	$4{,}09 \cdot 10^{-4}$	$2{,}17 \cdot 10^{-3}$	-
In116	$144.30 \cdot 10^{-3}$	$2{,}54 \cdot 10^{-4}$	$1{,}76 \cdot 10^{-3}$	$1{,}96 \cdot 10^{-4}$	$1{,}36 \cdot 10^{-3}$	-
In134	$51.27 \cdot 10^{-3}$	$5{,}00 \cdot 10^{-4}$	$9{,}76 \cdot 10^{-3}$	$3{,}06 \cdot 10^{-4}$	$5{,}97 \cdot 10^{-3}$	-
In413	$245.94 \cdot 10^{-3}$	$1{,}10 \cdot 10^{-3}$	$4{,}48 \cdot 10^{-3}$	$8{,}11 \cdot 10^{-4}$	$3{,}30 \cdot 10^{-3}$	-
In611	$71.54 \cdot 10^{-3}$	$4{,}14 \cdot 10^{-4}$	$5{,}78 \cdot 10^{-3}$	$2{,}76 \cdot 10^{-3}$	$3{,}86 \cdot 10^{-2}$	+
In431	$139.91 \cdot 10^{-3}$	$1{,}63 \cdot 10^{-3}$	$1{,}17 \cdot 10^{-2}$	$2{,}66 \cdot 10^{-3}$	$1{,}90 \cdot 10^{-2}$	+
In341	$153.37 \cdot 10^{-3}$	$1{,}47 \cdot 10^{-2}$	$9{,}56 \cdot 10^{-2}$	$2{,}75 \cdot 10^{-2}$	$1{,}79 \cdot 10^{-1}$	+
In161	$237.49 \cdot 10^{-3}$	$8{,}30 \cdot 10^{-2}$	$3{,}50 \cdot 10^{-1}$	$1{,}65 \cdot 10^{-1}$	$6{,}96 \cdot 10^{-1}$	+
In143	$115.05 \cdot 10^{-3}$	$3{,}01 \cdot 10^{-4}$	$3{,}67 \cdot 10^{-3}$	$2{,}77 \cdot 10^{-4}$	$2{,}41 \cdot 10^{-3}$	-
Po314	$66.61 \cdot 10^{-3}$	$5{,}06 \cdot 10^{-3}$	$7{,}59 \cdot 10^{-2}$	$5{,}92 \cdot 10^{-3}$	$8{,}89 \cdot 10^{-2}$	+

Po116	$61.10 \cdot 10^{-3}$	$1{,}59 \cdot 10^{-3}$	$2{,}61 \cdot 10^{-2}$	$2{,}06 \cdot 10^{-3}$	$3{,}37 \cdot 10^{-2}$	+
Po134	$73.83 \cdot 10^{-3}$	$4{,}08 \cdot 10^{-3}$	$5{,}53 \cdot 10^{-2}$	$5{,}43 \cdot 10^{-3}$	$7{,}35 \cdot 10^{-2}$	+
Po413	$76.97 \cdot 10^{-3}$	$1{,}09 \cdot 10^{-3}$	$1{,}41 \cdot 10^{-2}$	$1{,}52 \cdot 10^{-3}$	$1{,}98 \cdot 10^{-3}$	+
Po611	$28.01 \cdot 10^{-3}$	$2{,}49 \cdot 10^{-2}$	$8{,}90 \cdot 10^{-1}$	$3{,}86 \cdot 10^{-2}$	1,38	+
Po431	$66.59 \cdot 10^{-3}$	$1{,}33 \cdot 10^{-3}$	$2{,}00 \cdot 10^{-2}$	$1{,}78 \cdot 10^{-3}$	$2{,}68 \cdot 10^{-2}$	+
Po341	$63.41 \cdot 10^{-3}$	$4{,}00 \cdot 10^{-3}$	$6{,}30 \cdot 10^{-2}$	$4{,}76 \cdot 10^{-3}$	$7{,}51 \cdot 10^{-2}$	+
Po161	$48.19 \cdot 10^{-3}$	$1{,}62 \cdot 10^{-3}$	$3{,}36 \cdot 10^{-2}$	$2{,}05 \cdot 10^{-3}$	$4{,}26 \cdot 10^{-2}$	+
Po143	$69.06 \cdot 10^{-3}$	$2{,}02 \cdot 10^{-3}$	$2{,}93 \cdot 10^{-2}$	$2{,}01 \cdot 10^{-3}$	$2{,}90 \cdot 10^{-2}$	+

Table S5. Summary of overpotentials for all pentlandite samples "pre" and "post" stability tests normalized to ECSA and geometric area.

Sample	η_{ECSA} **[mV]**				η_{geo}	
Pellets	"pre" 25 [mA/cm²]	"post" 25 [mA/cm²]	"pre" 100 [mA/cm²]	"post" 100 [mA/cm²]	"pre" 10 [mA/cm²]	"post" 10 [mA/cm²]
Pe314	312.54	300.28	461.33	484.09	451.71	-
Pe116	-*	-*	69.21*	326.54	341.42	387.81
Pe134	364.18	378.18	-	-	466.59	422.82
Pe413	310.79	241.64	427.20	401.82	519.98	-
Pe611	309.91	415.82	-	-	219.76*	288.03*
Pe431	321.29	383.44	481.47	-	317.79	275.78
Pe341	401.82	418.45	-	-	379.93	320.42
Pe161	351.05	353.68	~244	-	285.40	288.03
Pe143	320.42	380.81	472.71	-	391.31	385.19
Ingots	"pre" 100 [mA/cm²]	"post" 100 [mA/cm²]	"pre" 500 [mA/cm²]	"post" 500 [mA/cm²]	"pre" 10 [mA/cm²]	"post" 10 [mA/cm²]
In314	248.64	309.91	441.20	424.57	-	-
In116	287.16	335.30	382.56	436.83	587.37	-
In134	295.91	262.65	411.44	514.73	556.74	-
In413	298.53	333.54	395.69	435.08	547.11	-
In611	296.78	400.07	358.05	-	527.86	-
In431	327.42	335.30	385.19	507.72	421.07	513.85
In341	460.46	566.37	-	-	464.84	444.70
In161	586.50	-	-	-	377.31	360.68
In143	475.34	519.10	-	-	-	-
Powders	"pre" 50 [mA/cm]	"post" 50 [mA/cm]	"pre" 250 [mA/cm]	"post" 250 [mA/cm]	"pre" 5 [mA/cm]	"post" 5 [mA/cm]
Po314	772.02	350.77	-	750.77	-794.77	357.02
Po116	833.27	818.27	-	-	-	-
Po134	832.02	740.77	-	-	-	770.77
Po413	457.02	388.27	550.77	477.02	580.77	477.02
Po611	877.02	-	-	-	614.52	728.27
Po431	817.02	830.77	-	-	-	-
Po341	534.52	568.27	698.27	813.27	567.02	594.52
Po161	710.77	845.77	810.77	-	773.27	-
Po143	570.77	684.52	694.52	819.52	660.77	789.52

Table S6. Tafel slope and j_0 (exchange current density) values of pentlandites samples "pre" and "post" stability tests.

Sample	ECSA "pre"		ECSA "post"		Geo "pre"		Geo "post"	
	Tafel slope [mV/dec]	J_0 [mA/cm^2]	Tafel slope [mV/dec]	J_0 [mA/cm^2]	Tafel slope [mV/dec]	J_0 [mA/cm^2]	Tafel slope [mV/dec]	J_0 [mA/cm^2]
Pe314	277	1222	281	1239	235	610	322	477
Pe116	113	931	91	715	92	486	86	513
Pe134	211	851	274	1012	214	589	263	688
Pe413	200	930	204	1013	196	564	198	380
Pe611	466	2179	406	1448	537	2055	423	1361
Pe431	204	920	205	828	214	789	210	860
Pe341	291	1010	275	955	297	823	281	912
Pe161	162	773	164	760	162	750	171	764
Pe143	239	1031	258	954	237	701	258	749
In314	250	1719	168	1068	257	461	167	382
In116	131	932	129	829	131	407	131	352
In134	142	932	303	1983	135	411	289	417
In413	133	854	134	858	134	400	142	397
In611	87	753	145	808	84	481	148	504
In431	75	665	153	935	78	476	151	511
In341	137	677	171	757	138	491	175	567
In161	156	709	175	697	159	603	177	656
In143	404	1917	450	2270	356	202	359	180
Po314	140	369	89	639	140	207	89	514
Po116	239	598	144	266	230	154	140	163
Po134	184	322	125	305	185	177	124	220
Po413	136	2	120	648	138	334	125	406
Po611	258	483	134	248	252	270	132	231
Po431	191	297	144	258	194	152	140	154
Po341	143	325	116	435	143	344	118	322
Po161	116	510	119	301	178	761	180	171
Po143	150	302	171	390	149	284	171	213

Table S7. Charge-transfer resistance determined by means of EIS.

Pellet		Ingot		Powder	
Sample	Resistance [Ω]	Sample	Resistance [Ω]	Sample	Resistance [Ω]
Pe314	14.87	In314	100.51	Po314	462.64
Pe116	8.01	In116	274.62	Po116	1200.09
Pe134	13.23	In134	190.12	Po134	361.89
Pe413	27.91	In413	101.31	Po413	863.72
Pe611	3.21	In611	111.65	Po611	228.51
Pe431	7.79	In431	64.87	Po431	815.16
Pe341	9.62	In341	70.28	Po341	371.86
Pe161	18.39	In161	19.39	Po161	364.75
Pe143	16.16	In143	56.57	Po143	40.18

Table S8. Comparison of achieved currents to previously tested materials.

Sample	η_{ECSA} [mV] 25 [mA/cm^2]
Pe314	313
Pe116	-*
Pe134	364
Pe413	311
Pe611	310
Pe431	321
Pe341	402
Pe161	351
Pe143	320
TM_9S_8 [17]	~270**
TM_9S_7Se [17]	~250**
$TM_9S_6Se_2$ [17]	~275**
$TM_9S_5Se_3$ [17]	~280**
$TM_9S_4Se_4$ [17]	~220**
$TM_9S_3Se_5$ [17]	~225**
$Ni_3Co_6S_8$ [15]	~350**
$Fe_{4,5}Ni_{4,5}S_8$ [15]	~350**
$Fe_3Co_3Ni_3S_8$ [15]	~325**
$Fe_3Co_2Ni_4S_8$ [15]	~360**
$Fe_3CoNi_5S_8$ [15]	~350**
$Fe_4Co_3Ni_2S_8$ [15]	~375**
$FeCo_5Ni_3S_8$ [15]	~375**
$Fe_2Co_4Ni_3S_8$ [15]	~350**
$Fe_{1.6}Co_{5.6}Ni_{1.8}S_8$ [15]	~360**

* See "3.3. $Co_{1,5}Fe_{1,5}Ni_6S_8$ phenomena"
** Values taken from the figures